A Microwave Quantum-Defined Millivolt Source

Akim A. Babenko, *Graduate Student Member, IEEE*, Nathan E. Flowers-Jacobs, *Member, IEEE*, Gregor Lasser, *Member, IEEE*, Justus A. Brevik, *Member, IEEE*, Anna E. Fox, *Senior Member, IEEE*, Paul D. Dresselhaus, Zoya Popović, *Fellow, IEEE*, and Samuel P. Benz, *Fellow, IEEE*

***Abstract*— We demonstrate a tenfold increase in the amplitude of microwave-frequency waveforms generated by a quantum-defined superconducting voltage source, with an open-circuit signal of 17.56 mV rms at 1.005 GHz. The voltage source is an RF Josephson arbitrary waveform synthesizer (RF-JAWS) that utilizes a circuit that is cooled to 4 K and is composed of an array of 4500 Josephson junctions. These junctions are connected in series along the center conductor of a 50-Ω superconducting coplanar waveguide transmission line. We introduce a new zero-forcing equalization technique for reducing distortion in drive current pulse patterns. This technique allows an increase in the amplitude of the quantum-based voltage waveforms while suppressing parasitic feedthrough signals to −75 dBc. Synthesizing a two-tone delta–sigma waveform, we monitor an audio-frequency 10-kHz tone of less than 100-μV rms amplitude while simultaneously measuring the 1.005-GHz tone of −28.12-dBm power in a 50-Ω environment. The two-tone synthesis allows simultaneous verification of correct operation of the voltage source using time-efficient low-frequency measurement techniques as well as slower microwave measurements.**

***Index Terms*— Equalizers, Josephson junctions (JJs), pulse measurements, superconducting integrated circuits, superconducting microwave devices.**

I. Introduction

PRIMARY RF power standards are based on a chain of detector standards, which are defined by calorimetry [1] and referenced indirectly to the quantum-SI-referenced system of standards. The RF Josephson arbitrary waveform synthesizer (RF-JAWS) is currently being developed [2], [3] as a quantum-based ac voltage source for RF and microwave metrology. Fig. 1 shows an RF-JAWS superconducting integrated circuit. The synthesizer will provide a new, quantum-SI-referenced arbitrary waveform source with high spectral purity and SNR for 4G [4], [5] and 5G [6] communications to complement the current calorimeter-based microwave power-calibration reference detectors. A dc-to-100-kHz JAWS is currently implemented as a primary standard for voltage metrology by the National Institute of Standards and Technology (NIST) [7], [8] and Physikalisch-Technisch Bundesanstalt (PTB) [9]–[11]. This primary standard is currently used to verify the performance of less accurate ac–dc thermal transfer standards [12]. The work presented in this article is a step toward expanding these low-frequency capabilities toward generating waveforms with useful amplitudes at microwave frequencies and achieving lower uncertainties than those provided by calorimeters [1], [13].

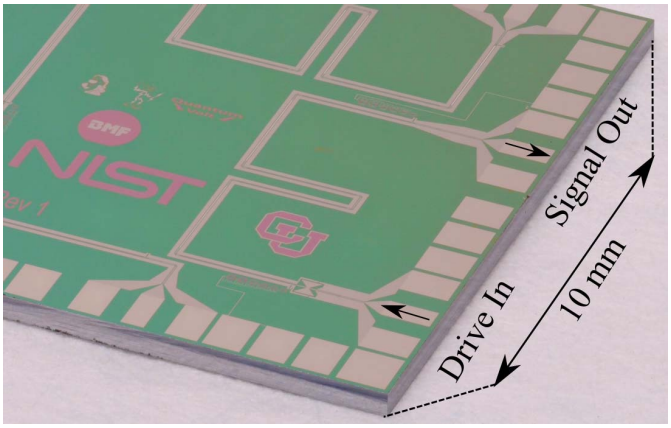

Fig. 1. Photograph of the 10 × 10 mm^2 chip with a 4500-JJ RF-JAWS test circuit marked with arrows indicating pulse signal flow. The rest of the chip is occupied by similar test circuits on its three other sides. "Drive In" is the drive current input. "Signal Out" is the voltage generated by JJs and the residual drive current output.

An RF-JAWS circuit consists of an array of thousands of Josephson junctions (JJs) operating at 4 K and is shown schematically in the top of Fig. 2. The JJs are embedded in a coplanar waveguide (CPW) transmission line of characteristic impedance Z_0. The JJs are driven by a pattern of current pulses I_{ac}, in this article at a rate of 14.4 Gpulses/s, which are added to a dc-bias current I_{dc} [14]–[16]. Within a range of drive current pulse shapes, amplitudes, and dc current magnitudes, each drive current pulse forces each JJ in the array to produce a single voltage pulse with a dc component of magnitude

Manuscript received April 17, 2021; revised June 5, 2021 and July 30, 2021; accepted August 28, 2021. Date of publication November 1, 2021; date of current version December 3, 2021. The work of Akim A. Babenko was supported by the National Institute of Standards and Technology (NIST) through the NIST-PREP Fellowship. The work of Zoya Popović was supported by the University of Colorado through the Lockheed Martin Endowed Chair in RF Engineering. *(Corresponding author: Akim A. Babenko.)*

Akim A. Babenko is with the Superconductive Electronics Group, National Institute of Standards and Technology (NIST), Boulder, CO 80305 USA, and also with the Department of Electrical, Computer and Energy Engineering, University of Colorado at Boulder, Boulder, CO 80309 USA (e-mail: akim.babenko@colorado.edu).

Nathan E. Flowers-Jacobs, Justus A. Brevik, Anna E. Fox, Paul D. Dresselhaus, and Samuel P. Benz are with the Superconductive Electronics Group, National Institute of Standards and Technology (NIST), Boulder, CO 80305 USA (e-mail: nathan.flowers-jacobs@nist.gov; justus.brevik@nist.gov; anna.fox@nist.gov; paul.dresselhaus@nist.gov; samuel.benz@nist.gov).

Gregor Lasser and Zoya Popović are with the Department of Electrical, Computer and Energy Engineering, University of Colorado at Boulder, Boulder, CO 80309 USA (e-mail: gregor.lasser@colorado.edu; zoya.popovic@colorado.edu).

Color versions of one or more figures in this article are available at https://doi.org/10.1109/TMTT.2021.3121425.

Digital Object Identifier 10.1109/TMTT.2021.3121425

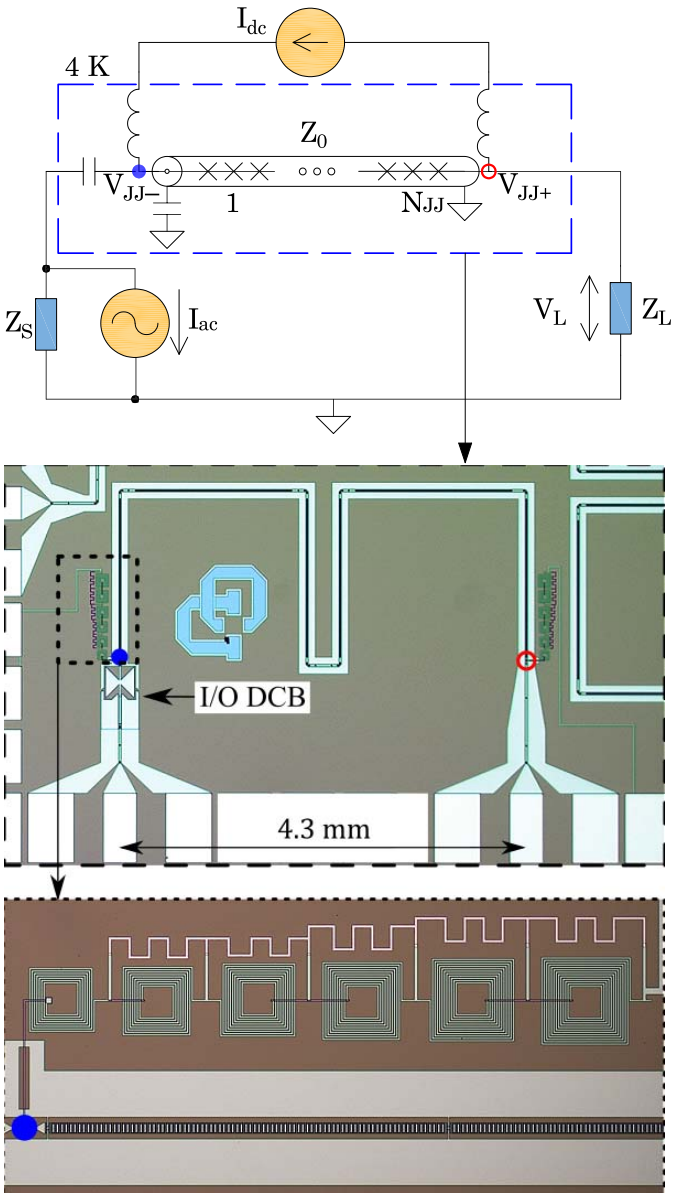

Fig. 2. Top: circuit diagram of an RF-JAWS, driven and biased by currents I_{ac} and I_{dc}. The × symbol denotes a JJ. Center: photograph of the on-chip RF-JAWS circuit shown in Fig. 1, with an $N_{JJ} = 4500$ JJ array. Bottom: detail of the on-chip inductors used for current bias and low-frequency voltage readout.

$h/2e$, where h is the Planck constant and e is the electron charge. This value is based solely on the quantum-mechanical properties of superconductors and $h/2e$ is a ratio of defined fundamental constants. The drive or bias range over which one drive pulse causes each JJ in the array to produce a single voltage pulse is defined as the quantum-locking range (QLR). The array generates a pulse that is a sum of the voltage pulses produced by each JJ in that array.

The drive current pulse shape and dc current magnitude do affect the shape of each JJ output voltage pulse. However, it is usually not practical to measure each voltage pulse in the time domain. Instead, a QLR is measured by determining that the synthesized dc or ac component of the voltage $V_{JJ} = (V_{JJ+} - V_{JJ-})$ (Fig. 2, top) across the array of N_{JJ} JJs remains effectively constant over a range of drive current pulse shapes, amplitudes, and dc-bias magnitudes. The error in the ac components of V_{JJ} associated with the nonzero pulsewidth of the output JJ voltage pulses is negligible for the synthesis frequencies used in this work [2].

In this work, we demonstrate that the RF-JAWS is operating correctly while generating voltage amplitudes not previously obtained; this is done by measuring QLRs while varying the drive current pulse amplitude and dc-bias current. We do not attempt to characterize the RF signal paths to the JJ array reference plane [17], [18]. Therefore, we assume a 50-Ω environment ($Z_S = Z_L = 50\ \Omega$) that the impedance of the JJ array is negligibly small up to 1 GHz when calculating the power generated by the JJ array [2], [3], [19].

Increasing the amplitude of the voltage waveforms generated by RF-JAWS provides higher SNR and spurious-free dynamic range (SFDR). This can be done by increasing either the number of JJs in an array or the pulse-repetition rate of the drive current I_{ac}. The former is limited by the loss that results from the normal-state resistance of the JJ array, while the latter is limited by the distortion and available bandwidth of the room-temperature and cryogenic paths of the drive current signal. The 4500 JJs in the nominally 50-Ω transmission line used in this work is the largest number of junctions to date for which microwave-frequency waveforms and QLRs have been demonstrated [2], [3], [17], [19].

To compensate for the distortion of the drive current signal, one needs to modify the shape of the pulses, which have about 20-GHz instantaneous bandwidth and several volts of peak-to-peak amplitude. Previous solutions achieved limited distortion mitigation using a real-time digital adaptive finite impulse response (FIR) filter [20], [21], with no direct measurements of the drive current pulse shape. The metric used for pulse distortion was the JAWS dc-bias-current QLR, which increases as the distortion is reduced. The approach was successfully used for microwave-frequency synthesis, but with limited pulse-repetition rates and thus limited synthesized voltage amplitude [2], [3]. In this work, we obtain a 20-dB increase in the synthesized microwave voltage/power by using increased drive current pulse-repetition rates, enabled by a new zero-forcing equalization technique.

Drive current at the synthesis frequency creates a parasitic "feedthrough" voltage that adds coherently to the quantum-based JJ voltage signal, through Z_L and any nonzero series impedance on the JAWS transmission line [see Fig. 2 (top)]. We substantially reduce this error at the relevant synthesis frequencies up to 1 GHz by using high-order high-pass filtering and equalize the resulting distorted drive current.

This article is organized as follows. In Section II, we review the JAWS operation principles, waveform generation, and on-chip circuitry. In Section III, we introduce the JAWS drive current electronics and describe in detail the zero-forcing equalization of the drive current pulses. Finally, in Section IV, we use these equalized drive pulses to generate a quantum-based −28-dBm 1.005-GHz waveform and confirm that the RF-JAWS is operating correctly by measuring the QLR with

respect to both drive current pulse amplitude and dc current. These QLR measurements use a new time-efficient measurement technique in which a two-tone waveform is generated with a small 88-μV 10-kHz tone as well as the large 18-mV 1.005-GHz tone, and the QLRs are simultaneously measured with low-frequency and microwave instruments.

II. Quantum-Based Voltage Generation

In this section, the dynamics of a JJ are first reviewed in the context of arbitrary voltage waveform generation. This introduction is followed by a description of JJ-based voltage synthesis of voltage waveforms up to 1 GHz and how the synthesized amplitudes can be precisely calculated from quantum-mechanical principles. Finally, we detail RF-JAWS circuit design, as well as the niobium (Nb) superconducting technology used for chip fabrication.

A. Dynamics of JJs

A JJ is made by creating a weak link between two superconductors [22]. The quantum-based superconducting properties of a JJ ensure that the device produces dc-quantized voltage pulses in response to a drive current through the JJ, if that drive current is greater than its critical current I_c. The time-integrated area of each voltage pulse is exactly equal to the magnetic flux quantum $\Phi_0 = h/2e$, where h is the Planck constant and e is the electron charge [22].

For JAWS, the drive current is composed of a pattern of pulses I_{ac} that is clocked at a rate of f_{clk}, which is combined with a dc-bias current I_{dc} [Fig. 2 (top)] [14], [16]. Within ranges of drive current pulse shapes and dc bias, a JJ converts each drive current pulse in the pattern I_{ac} into a single voltage pulse. We call such ranges the QLRs for a particular drive or dc-bias-current parameter. Within a QLR, the drive current pulse shape and dc bias affect the timing and shape of the JJ output pulse [2], [23]. However, this has a negligible effect on the power and spectral purity at the synthesis frequencies up to 1 GHz used in this work.

While the dc value of each JJ voltage pulse is exactly equal to Φ_0, the fabrication process determines I_c, normal resistance R_n, and capacitance C of the JJ. These parameters establish requirements for the drive current as well as impose limitations on the JJ voltage pulse shape. The JJs used in this work have $I_c = 9.5$ mA, $R_n = 4$ mΩ, and negligible capacitance of $C < 0.1$ pF. The normal resistance R_n shunts the junction and thus does not affect the voltage across it. However, the resistance affects the JAWS circuit in two ways. First, it causes dissipation of the drive current pulses I_{ac} when the JJ produces voltage pulses, which limits the number of JJs that can be driven in series. Second, it low-pass (LP) filters I_{ac} with an RL-type characteristic frequency $f_c = I_c R_n/\Phi_0$ [22]. The characteristic frequency of the junctions in this article is $f_c = 18$ GHz. When the half-peak pulsewidth is comparable to $1/f_c$, the required drive current pulse peak amplitude to force the JJ to pulse is $2.6I_c$ [15].

B. Delta–Sigma Voltage Waveforms of Calculable Amplitude

The synthesized voltage waveform $V_{JJ}(t)$ is determined by the drive pulse pattern I_{ac} and number of JJs, N_{JJ}. When I_{ac} is composed of pulses at a constant repetition frequency f_{clk}, the junctions produce a frequency comb at multiples of f_{clk} with a dc voltage $V_{JJ}^{dc} = N_{JJ} f_{clk} \Phi_0$. Generating arbitrary waveforms is typically accomplished by using the delta–sigma modulation. At each delta–sigma time step $T_{clk} = 1/f_{clk}$, all the JJs produce a positive pulse, for drive current pulse corresponding to a $+1$ symbol in the delta–sigma code, a negative pulse (-1), or no pulse (0). This approach can synthesize high-SNR signals using a limited number of pulse output levels [24], in this case three, while minimizing the associated digitization noise within some bandwidth around a synthesis frequency f_t. A delta–sigma modulator is a feedback loop that shapes this digitization noise with a noise transfer function (NTF) that has a notch around f_t. LP delta–sigma modulation has been used to encode waveforms from dc to 100-kHz [8], [14], [16] JAWS, and bandpass (BP) delta–sigma modulation has been used for RF [2], [3], [17]. The highest f_t synthesis frequency is limited primarily by the highest available f_{clk} and the feedback parameters of the delta–sigma modulator [24]. f_t has a resolution limited by the number of samples in the delta–sigma pattern and the resolution of f_{clk}. Therefore, the resolution of f_t is practically limited by the phase noise of the drive current instrumentation.

The synthesized voltage waveform can be calculated from the pulse sequence $w[n]$ ($n \in \mathbb{Z}$) and the shape of each pulse $P(t)$. For $w[n]$ taking one of the three levels (-1, 0, 1) at each n and $P(t)$ with a dc component of unity, the output voltage across a series array of N_{JJ} junctions is

$$V_{JJ} = N_{JJ}\Phi_0 \; P(t) \otimes \sum_n w[n]\delta(t - nT_{clk}) \tag{1}$$

where $\otimes$ is the convolution operator and δ is the Kronecker delta function [23]. The finite width and shape of the combined voltage pulses $N_{JJ}\Phi_0 \; P(t)$ is a source of error in calculating V_{JJ} and depends on the shape of the drive current pulses I_{ac}, the dc-bias current I_{dc}, the characteristic frequency f_c, and the length of the JJ array. For the JJs and array in this article, this error is negligible for synthesis frequencies up to about 1 GHz [2], which is the highest value used in this work.

The drive current creates a systematic feedthrough error voltage that is coherent with V_{JJ} when it passes through the impedances in the RF-JAWS signal path. We reduce this error by attenuating the power at the synthesis frequency f_t in the drive signal. When using three-level (-1, 0, 1) drive current pulse shapes [Fig. 3(a)], the frequency content of the drive signal closely matches that of the JJ output voltage [Fig. 3(c), solid]. To reduce this error, we digitally high-pass filter (HPF) the pulse drive by using the five-level (-1, -0.5, 0, 0.5, 1) drive pulse shapes in Fig. 3(b). For these pulse shapes, the central, unity-area, ± 1 pulse is surrounded by two half-area ∓ 0.5 pulses. This reduces the drive signal power at f_t by more than 30 dB at frequencies up to 1 GHz [Fig. 3(c)]. Due to the JJ nonlinearity, only the central ± 1 drive current pulse is sufficiently above I_c to force each JJ to create a voltage pulse with integrated area Φ_0. The half-area ± 0.5 pulses do not cause the JJs to pulse and perform only high-pass filtering of the drive current.

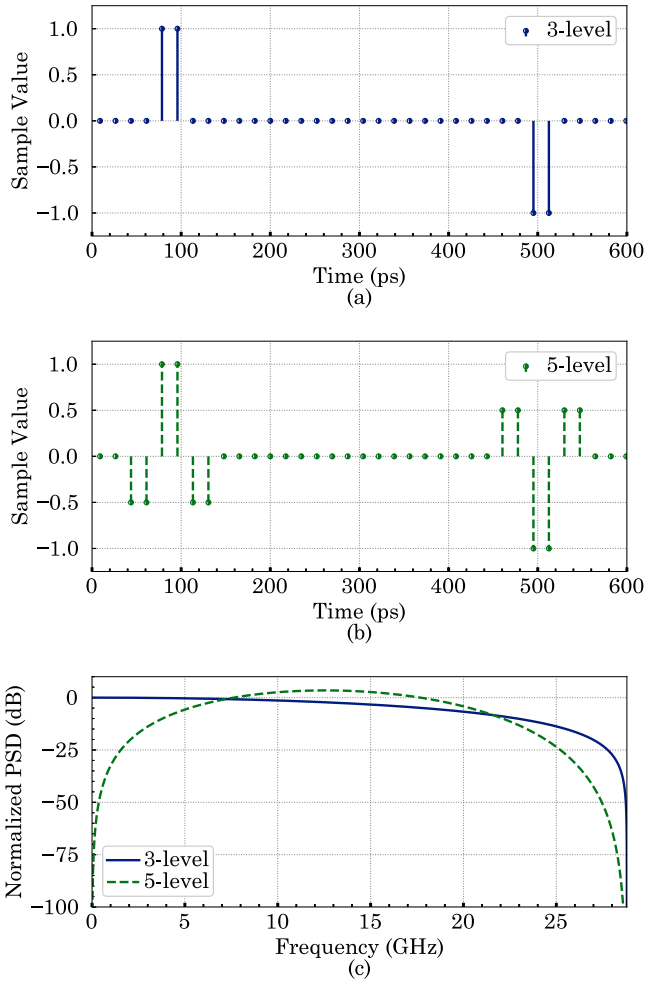

Fig. 3. Illustration of (a) three- and (b) five-level pulses at the experimental 57.6-GSa/s sampling rate, where each symbol is two samples' wide. (c) Corresponding spectra of single positive three-level (blue solid line) and five-level (green dashed line) pulses. The PSD plots have been normalized to the dc component of the three-level pulse.

In this work, we synthesize two-tone waveforms containing both audio- and microwave-frequency components. The delta–sigma NTF is a convolution of a BP NTF centered around 1.005-GHz and an LP NTF (Fig. 4, blue dashed line). We use this NTF to calculate a pulse pattern comprising 28.8 million samples at 57.6 GSa/s that generates V_{JJ} of 0.088 mV at 10 kHz and 17.564 mV at 1.005 GHz with a 4500-JJ array. We chose a synthesis frequency of 1.005 GHz to avoid intermittent spurs observed in the measurement setup at 1 GHz. The choice of 10 kHz is convenient for low-frequency RF-JAWS QLR measurements. The calculated JJ output three-level spectrum is shown in Fig. 4 (green), where it has been normalized to the 1.005-GHz tone. The spectrum using the five-level pulses [Fig. 3(b)] is shown in red, which shows a reduction in power of more than 30 dB up to 1.005 GHz. However, a drive current pulse across $Z_L = 50\ \Omega$ typically produces 10-dB higher peak amplitude than the typical 4500-JJ voltage pulse, with a similar difference at f_t. This necessitates analog high-pass filtering to further reduce the signal at f_t in the drive signal and thus further suppress the feedthrough error voltage.

C. RF-JAWS On-Chip Circuit

On-chip RF-JAWS circuits have been implemented as one-port [17] and two-port [2], [19] networks. The one-port circuit consists of series-connected JJs on the center conductor of a CPW line, with a pulse input–output port on one side of the CPW and an on-chip termination resistor Z_L on the other [2], [18]. The two-port circuit has a drive current input port on one side of the CPW and an output voltage port on the other [2]. Using an on-chip termination resistor results in a better broadband match for the drive current and voltage pulses. However, the measured backward-propagating JJ voltage pulses are broadened [25] and it is more difficult to direct them to a device under test (DUT) or a measurement instrument.

In this work, we use a two-port RF-JAWS circuit (Fig. 2). Since we measure the voltage pulses on the port opposite the drive port, the voltage pulses copropagate with the drive current pulses and therefore are not broadened [25]. Z_L, in this case a room-temperature measurement instrument, is connected to the output of the JJ array via minimal off-chip components. Unfortunately, these off-chip components do increase the drive current voltage standing-wave ratio (VSWR) compared to the on-chip termination of a one-port RF-JAWS circuit. This also leads to interpulse interference along the array that reduces the QLR. For this reason, earlier two-port RF-JAWS networks required on-chip matching/filtering components and lower pulse-repetition rates to achieve sufficient QLRs (greater than 1 mA of dc-bias current) [2]. The drive current equalization technique introduced in this article allows the use of a simpler two-port RF-JAWS circuit without additional on-chip components and at higher pulse-repetition rates.

The chip used in this article (Figs. 1 and 2) was fabricated using superconducting Nb materials [26] on an oxidized 350 μm undoped silicon (Si) substrate ($\varepsilon_r = 12$). The JJs were made by placing a 30-nm metallic layer of Nb_xSi_{1-x} between two layers of niobium, with a junction area of 50 μm^2. The JJs are embedded in the center conductor of a Nb CPW. The process has two Nb layers—wiring (WR) and base electrode (BE)—separated by 300 nm of silicon dioxide (SiO_2) with a superconducting via interconnect. The CPW characteristic impedance is designed to be 50 Ω, with the center conductor width $w = 16\ \mu$m and gap $g = 8\ \mu$m. The loading of the CPW line by the 4500 JJs is negligible for $f_t \leq 1$ GHz, given the values of I_c and R_n used in this work [22]. The effective dielectric constant is $\varepsilon_{\text{eff}} = 5.98$. Thus, a 1-mm CPW line is a quarter-wave long at 30.6 GHz, with a total delay $t_d = 8.16$ ps. The drive current input is followed by an inside/outside dc block (Fig. 2) to isolate the signal/ground dc and low-frequency currents from the room-temperature electronics [19], [27]. A set of series-connected inductors is implemented to bias and measure dc and low-frequency voltage [27] across the JJ array. The RF-JAWS superconducting circuit was operated in liquid helium, which has a temperature

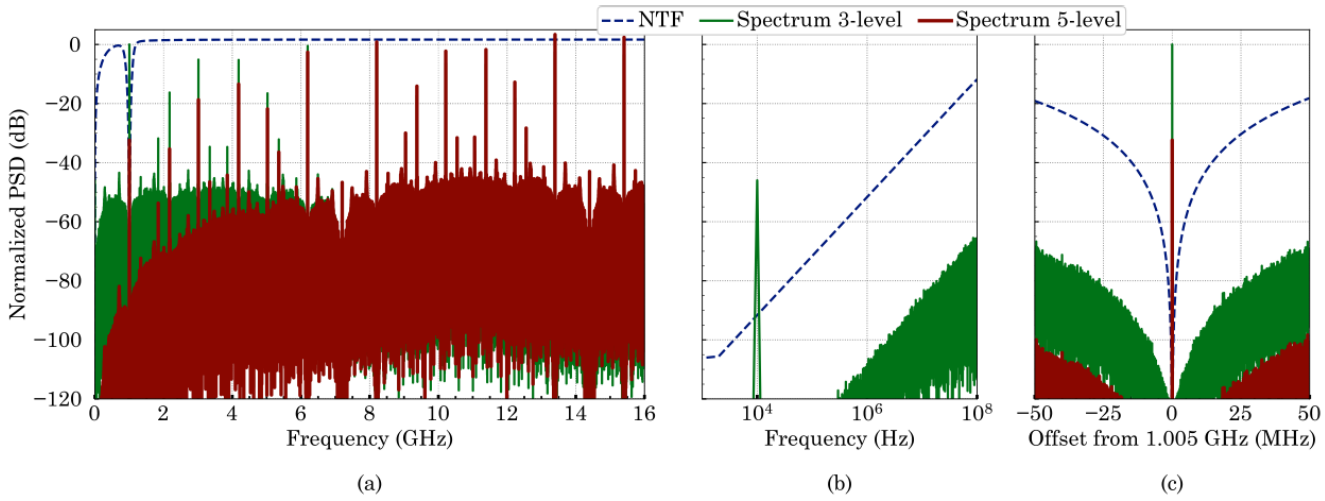

Fig. 4. NTF and spectra of three- and five-level bipolar delta–sigma patterns with tones at 10 kHz and 1.005 GHz. (a) NTF and spectra up to 16 GHz. (b) and (c) Parts of the spectra in (a) around 10 kHz and 1.005 GHz on logarithmic and linear frequency scales, respectively. Each delta–sigma pulse is shown in Fig. 3, with at least two zeros around each symbol, which results in a delta–sigma modulation clock frequency of 14.4 GHz. The amplitudes of the tones synthesized in the digital code are adjusted to produce 0.088-mV rms at 10 kHz and 17.564-mV rms at 1.005 GHz, for a 4500-JJ array. The spectra are normalized to the 17.564-mV peak at 1.005 GHz.

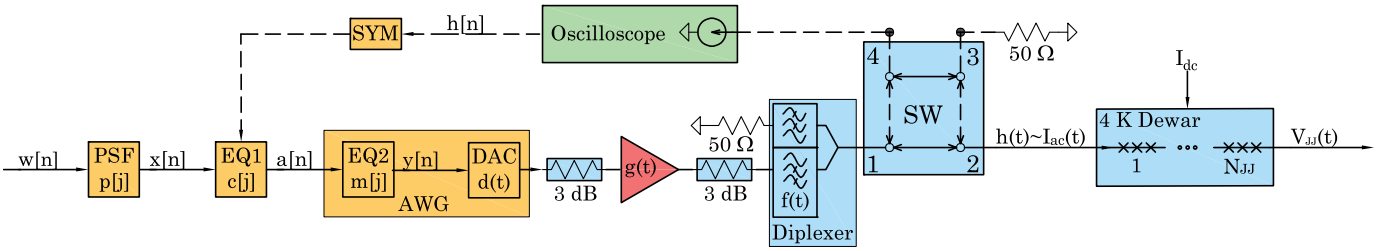

Fig. 5. RF-JAWS mixed-signal generation and processing block diagram. Dashed lines denote off-line signal flow. The DAC with impulse response $d(t)$, amplifier $g(t)$, and HPF $f(t)$ is used to generate and process analog delta–sigma pulses $h(t)$ that are proportional to the drive current $I_{\rm ac}$. The DAC and EQ2 are built into the AWG. The oscilloscope and switch (SW) are used to sample the analog signal $h(t)$ for further processing in the symmetrization block SYM. The pulses $h(t)$ drive an array of N_{JJ} JJs biased with $I_{\rm dc}$ to generate quantum-based arbitrary voltage waveforms V_{JJ}.

of 4.0 K at the elevation of 1600 m above the sea level where our measurements took place.

III. Drive Current Equalization

If the drive current pulse shape is too distorted, the JJs will either fail to generate pulses or will generate extraneous pulses, and therefore, the QLR will be nonexistent. In this section, the drive current digital and analog signal processing schemes are described. A new approach to equalization is then presented. We quantify the distortion with the fidelity factor FF [28], wich is often used for ultrawideband antennas. This maximum cross correlation between two digital signals $u[n]$ and $v[n]$, with respect to the time/sample delay k between them, is defined as

$$\mathrm{FF}(u,v)=\max_k\left|\frac{\sum_n u[n]v[n-k]}{\sqrt{\sum_n|u[n]|^2\sum_n|v[n]|^2}}\right|. \tag{2}$$

FF is normalized by the product of the norms of the two signals, and its value is between 0 and 1, where FF = 1 for two identical signals, and smaller values correspond to larger discrepancies between the two. FF can also be used to find the sample delay k between two waveforms with the same sequence of pulses, but with different distortion [29].

A. Drive Current Signal Path

The mixed-signal drive current path is shown in Fig. 5. First, the delta–sigma algorithm is used to generate a three-level pulse sequence $w[n]$. The pulse-shaping filter (PSF) and equalizers EQ1 and EQ2 are FIR filters [30] with coefficients (taps) $p[j]$, $c[j]$, and $m[j]$ ($j\in\mathbb{Z}$), respectively. The pulse sequence $w[n]$ is converted into five-level pulses $x[n]$ using the PSF to reduce the feedthrough voltage as described in Section II.

A Keysight M8195A arbitrary waveform generator (AWG)[1] implements the equalizer EQ2 and digital-to-analog converter (DAC) (Fig. 5). The drive current waveform is generated at a 57.6-GSa/s sampling rate (as in Fig. 3). The generator has a 3-dB analog signal bandwidth of about 25 GHz, and an internal real-time digital FIR filter EQ2 with 16 taps $m[j]$ (Fig. 5) spaced at 57.6 GSa/s. Thus, EQ2 is a fractionally

[1]Commercial instruments and devices are identified in order to adequately specify the experimental procedure. Such identification does not imply recommendation or endorsement by NIST nor does it imply that the equipment identified is necessarily the best available for the purpose.

spaced equalizer [31] for the five-level pulses in Fig. 3. Based purely on low-frequency JAWS QLR measurements, we perform additional equalization manually using the coefficients $m[j]$. This results in the samples $y[n]$, which are applied to the input of the 8-bit zero-order hold (ZOH) DAC. The additional tuning with $m[j]$ compensates for drive current distortion occurring in the room-to-cryogenic temperature signal path.

The maximum AWG output amplitude of $1\,V_{p\text{-}p}$ is insufficient to drive the JJ array. Commercially available GaAs distributed amplifiers [32], [33] ($g(t)$ in Fig. 5) amplify the drive current pulses with about 25 GHz of instantaneous bandwidth. We built a three-stage amplifier using three printed circuit boards (PCBs) from XMicrowave with MACOM MAAM-011109, ADI HMC994APM5E, and ADI HMC998APM5E in the first, second, and third stages, respectively. The amplifier provides around 32-dB small-signal gain from 10 MHz to 22 GHz, with a 3-dB gain roll-off around 24 GHz. This is sufficient bandwidth to amplify the drive current pulses [Fig. 3(c)]. The amplifier has an average 1-dB compression point of 1 W, that is, 140 mA into 50 Ω, across the frequency range. The 3-dB attenuator before the amplifier extends the usable dynamic range of the AWG by moving the usable sweep of the AWG amplitude.

Nonlinearities of the amplifier ($g(t)$ in Fig. 5) can downconvert or upconvert the delta–sigma tones located at $jf_{\text{clk}} + kf_t$, with $j, k \in \mathbb{Z}$ and $j, k \neq 0$ [e.g., tones at 14.4 ± 1.005 GHz in Fig. 4(a)]. Some of these intermodulation distortion (IMD) products occur at the synthesis frequencies f_t and contribute to the feedthrough error. We reduce this error by using the analog HPF of a Mini-Circuits ZDSS-3G4G-S+ diplexer, which has a nominal cutoff frequency of 3.4 GHz. The HPF port was connected to the amplifier and the combined (COM) port was connected to the JJ array via the room-to-cryogenic temperature signal path. The low-pass filter (LPF) port was terminated with a coaxial 50-Ω resistor.

After the diplexer (Fig. 5), a switch (SW) directs the drive pulse sequence $h(t)$ to either a sampling oscilloscope (Agilent 86100C, with an 86117A 50-GHz dual-channel module) in the dashed position or the top of a liquid helium dewar in the solid position of SW. The symmetrization block (SYM) is used to calculate the coefficients c[j] for equalizer EQ1. The oscilloscope impulse response is assumed to be ideal within the 28.8-GHz equalization bandwidth. The SW block is a Keysight 87222D transfer switch with 0.2-dB average insertion loss over 100 dB of isolation and <0.03-dB insertion loss repeatability. We use nominally identical cables on ports 2 and 4 of SW. The components beyond the top of the dewar cause linear distortion of the drive current pulses I_{ac} at the JJ array compared to $h(t)$, which is compensated by tuning the $m[j]$ taps of EQ2.

B. Drive Current Zero-Forcing Symmetrization

We use an equalizing FIR filter EQ1 with coefficients $c[j]$ to symmetrize the five-level drive current pulses. The band-limited analog signal path containing the dispersive HPF mainly affects the second half of the pulse (e.g., [34, Fig. 3(c)]). We measure an initial pulse shape $h(t)$ with equalizers EQ1 and EQ2 deactivated ($c[j] = m[j] = \delta[j]$) and create a target pulse shape by mirroring the first half of $h(t)$ about the main peak. We then perform zero-forcing equalization [35] to find the taps $c[j]$ that symmetrize the measured $h(t) \propto I_{\text{ac}}(t)$.

The symmetrized version of the measured pulse is used as the target pulse shape for the following reasons.

1) We mainly require that each drive current pulse causes each JJ to generate a voltage pulse and that the dc component of the five-level pulse is zero—a particular pulse shape (rectangular, raised cosine, Gaussian, and so on) is not required.
2) The limited AWG sampling rate of two samples per symbol does not easily support the generation of different pulse types.
3) A symmetrized pulse shape accommodates the limited bandwidth of the signal path.
4) We have found experimentally that the small distortion before the main peak can be neglected for driving the JJs.

The zero-forcing algorithm is described next with intermediate steps shown in Fig. 6.

1) Create a test pattern $w[n]$ composed of a single positive pulse (two samples at $f_s = 57.6$ GSa/s), with the PSF $p[j]$ set to the five-level pulse shape and the other filters $c[j]$ and $m[j]$ set to $\delta[j]$, so that $x[n] = a[n] = y[n]$.
2) Generate the pattern using the AWG with programmed peak-to-peak AWG amplitude of $0.325\,V_{p\text{-}p}$.
3) Measure the pulse $h(t)$ (Fig. 6(a), blue solid) at the top of the liquid helium dewar at a sampling rate of $8 \times f_s$.
4) Calculate the target pulse shape by symmetrizing the measured signal $s(h(t)) = h(-|t|)$ (Fig. 6(a), green dashed), where $t = 0$ corresponds to the location of the first maximum of the single positive pulse.
5) Calculate the equalization coefficients $c[j]$ by solving the convolution equation $s(h[n]) = h[n] \otimes c[j]$ in the frequency domain.
   a) Zero-pad 2^{11} samples of 4.4 ns of $h(t)$ and $s(h(t))$ with 2.5×2^{14} samples, creating a 100 ns waveform with 10 MHz frequency resolution.
   b) Downsample the measured pulse shape $h(t) \rightarrow h[n]$ down to f_s, with $h(0) = h[0]$.
   c) Use discrete Fourier transforms (DFTs) $DFT[h[n]] = H[\omega]$ and $DFT[s(h[n])] = S(h)[\omega]$ to calculate $c[j]$ in the frequency domain $C[\omega] = S(h)[\omega]/H[\omega]$ and then set the filter $C[\omega]$ to unity (ZOH) below 3.45 GHz and above 21.5 GHz [Fig. 6(b)].
   d) Obtain $c[j]$ as the inverse DFT of $C[\omega]$.
6) Use $c[j]$ to generate an improved drive current pulse and compare a measurement of the new pulse $h'(t)$ to the calculated nondecimated expectation $(h[n] \otimes c[j])(t)$ at $8 \times f_s$ using FF as the distortion metric [Fig. 6(c)].

The algorithm increases FF from 85.5% for the measured distorted pulse $h(t)$ to 97.8% for the calculated equalized pulse $((h[n] \otimes c[j])(t))$, when both are compared to the initial target $s(h(t))$. Since the RF amplifier is operating near saturation,

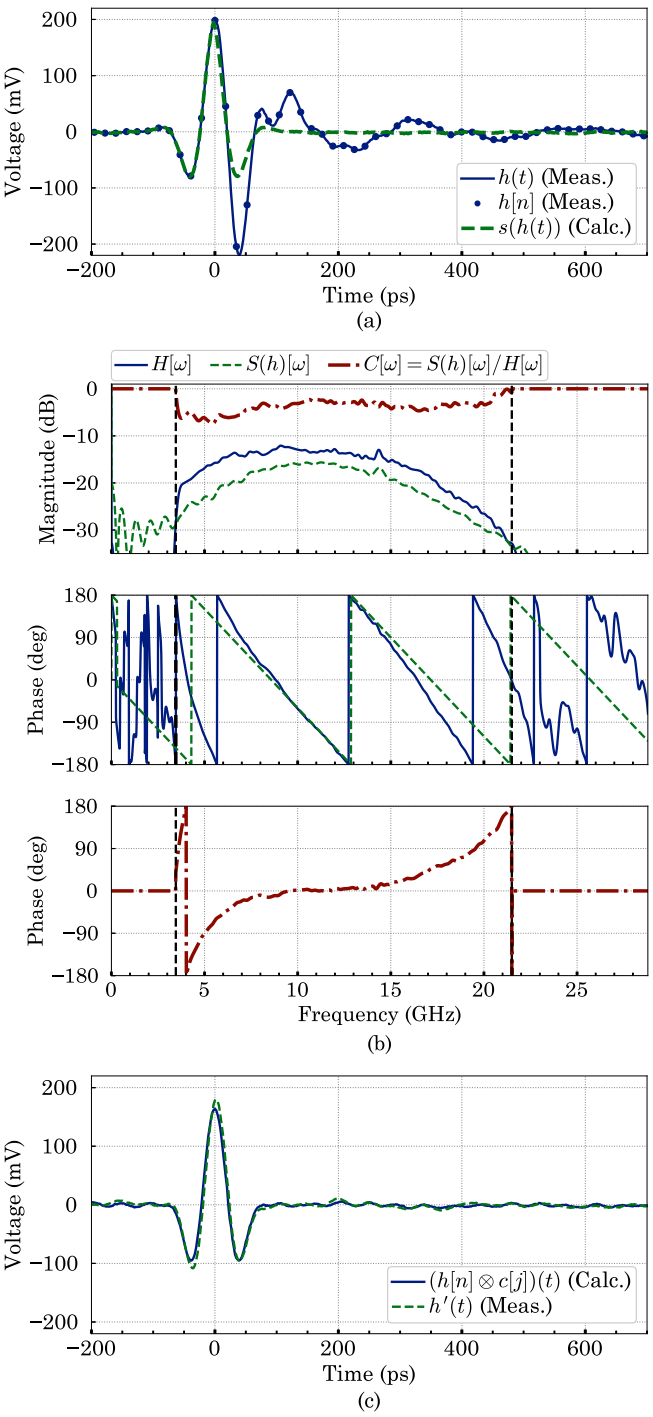

Fig. 6. (a) Measured distorted [blue solid, $h(t)$] pulse at the input of the cryostat and calculated symmetrized [green dashed, $s(h(t))$] pulse. (b) Discrete Fourier transforms (DFTs) of the measured distorted (blue solid) and calculated symmetrized (green dashed) pulses, as well as their ratio (red dashed-dotted). Zero-forcing symmetrization of five-level pulses. A single pulse $h(t)$ is measured at the input of the cryostat [blue solid pulse in (a) and DFTs in (b)] and then symmetrized [$s(h(t))$ green dashed pulse in (a) and DFTs in (b)], and the ratio in the frequency domain is calculated to determine the equalizing filter $c[j]$ [red dashed-dotted DFTs in (b)]. (c) Calculated [$(h[n] \otimes c[j])(t)$, blue solid] and measured ($h'(t)$, green dashed) equalized pulses. The equalizing filter is used from 3.45 to 21.5 GHz [vertical dashed lines in (b)]. In (b), the DFTs of $S(h)[\omega]$ and $H[\omega]$ are offset up by 35 dB and a 1.2-ns delay is subtracted from the DFTs for clarity.

the measured equalized pulse $h'(t)$ deviates from $s((h(t))$ (FF = 97.4%); this cannot be linearized. It is possible to improve FF by iterating over the algorithm above or by using

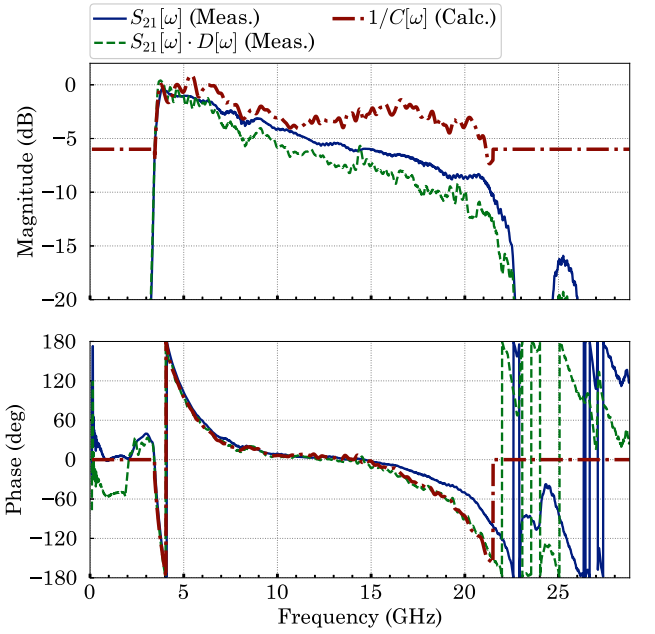

Fig. 7. Measured S_{21} magnitude and phase of the signal path: the amplifier, HPF, and intermediate interconnects (blue solid); combined with the AWG frequency response $D[\omega]$ (green dashed); and compared to the inverse equalizer in the frequency domain $1/C[\omega]$ (dashed-dotted red). For comparison, the magnitudes of S_{21}, $S_{21} \cdot D[\omega]$, and $1/C[\omega]$ are offset by -30, -26, and -6 dB, respectively. The measured S_{21} and $D[\omega]$ phases are desloped by subtracting delays of 8.7 and 3.1 ns, respectively.

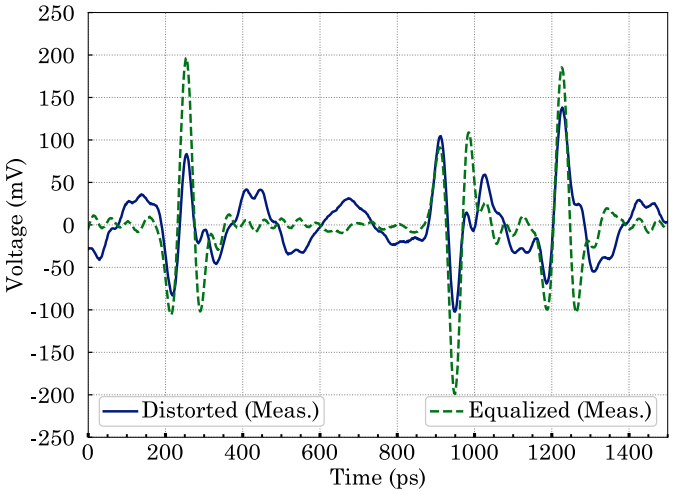

Fig. 8. Distorted (blue solid) and symmetrized/equalized (green dashed) five-level drive current pulses, which were both measured at the input of the cryostat at a sampling rate of 8×57.6 GSa/s.

nonlinear equalization [36], [37]. However, the single iteration is sufficient to reduce most of the distortion.

Although the zero-forcing equalization procedure above does not require any knowledge of the room-temperature analog signal path, we can understand the main sources of distortion by measuring the frequency response. The scattering (S-) parameters of the signal path between the AWG and the dewar (Fig. 5, solid position of SW) are measured with a vector network analyzer (VNA; Agilent E8364B) and are shown in Fig. 7 (blue solid line). The frequency response

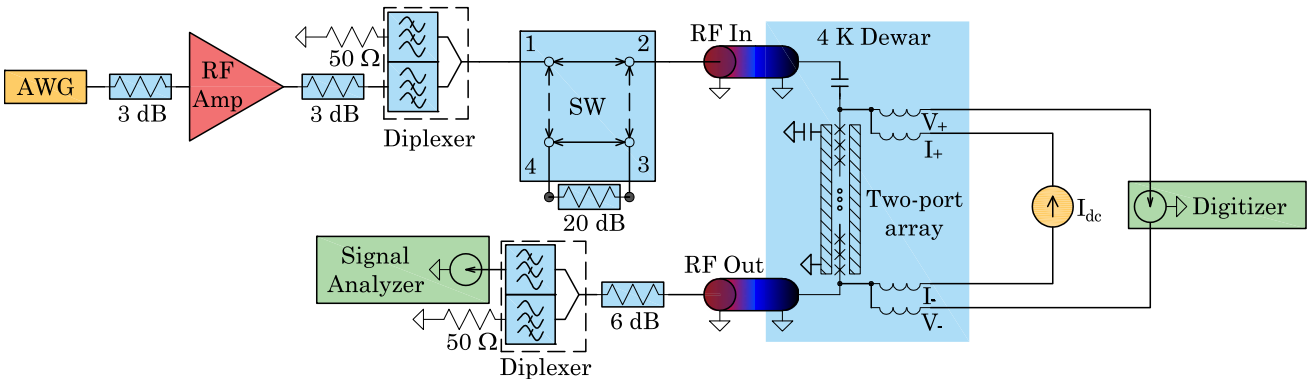

Fig. 9. Diagram of the QLR measurement setup, which is used to verify the RF-JAWS operation. The AWG outputs the delta–sigma patterns, which are then amplified and filtered. Ports 3 and 4 of the SW can also be connected to a 20-dB attenuator to measure the feedthrough signal (dashed position). The "RF In" and "RF Out" coaxial cabling is exposed to the room-to-cryogenic temperature gradient. The synthesized audio-frequency voltage is measured across the array with the digitizer and the dc current bias is applied using a current source I_{dc}, in a four-probe configuration. At the RF output, synthesized microwave tones are measured with the signal analyzer after attenuation and LP filtering.

of the AWG is determined by connecting the oscilloscope directly to the output of the AWG. The AWG is loaded with a single positive pulse as in step 1 of the algorithm mentioned above $h_{\mathrm{AWG}}(t) = x[n]\Pi(t - nT_s) \otimes d(t)$, where $T_s = 1/f_s$ and $\Pi(t)$ is the rectangular or ZOH function. The AWG frequency response is thus $D[\omega] = DFT(h_{\mathrm{AWG}}(t))/DFT(x[n]\Pi(t - nT_s))$, where the $x(t)$ pulse is scaled to have the peak amplitude of $h_{\mathrm{AWG}}(t)$. The frequency response $S_{21}[\omega] \cdot D[\omega]$ of the analog signal path is plotted in Fig. 7 (green dashed line).

The coefficients $c[j]$ that symmetrize the five-level pulse (Figs. 6 and 7, red dashed-dotted) are consistent with the measured characteristics of the AWG and analog components (Fig. 7, green dashed line). The magnitude discrepancy increases above 10 GHz because the symmetrization procedure does not correct for the intrinsic LP roll-off of the analog signal path. The phases agree to be within $\pm 15°$ over the relevant frequency range from 3.45 to 21.5 GHz. The dispersive phase response of the signal path is therefore the main cause of the pulse asymmetry. For a new $C'[\omega]$ with $|C'[\omega]| = 1$ and only $\angle C'[\omega]$ used, FF between the calculated pulse $(h[n] \otimes c'[j])(t)$ and the symmetrized version $s(h(t))$ is 97.1%.

IV. Quantum-Locking Range Measurements

To demonstrate that the RF-JAWS source is operating correctly, we measure QLRs for the two-tone delta–sigma pattern shown in Fig. 4, which generates tones across the 4500-JJ array of 0.088-mV rms at 10 kHz and 17.564-mV rms at 1.005 GHz. The programmed digital waveform is 500 μs or 28.8 million samples long, comprising five 10-kHz periods and 502 500 1.005-GHz periods. This waveform length allows the delta–sigma algorithm to achieve a calculated average SFDR of 99 dBc within a bandwidth of 10 MHz around 1.005 GHz.

The EQ1 $c[j]$ coefficients determined in Section III are convolved with the drive current pulses in the two-tone delta–sigma waveform, with no additional iterations of the symmetrization algorithm. In Fig. 8, the initial distorted drive current pulses (blue solid line) are compared to the symmetrized pulses (green dashed line). We show a fraction of the total waveform spanning 1.5 periods at 1.005 GHz. Given the observed difference, it is not surprising that the distorted pulses are unable to cause the JJs to pulse appropriately. In contrast, the symmetrized pulses show negligible interpulse interference.

A JAWS QLR is defined as the range of any drive, bias, or environmental parameter over which each JJ generates exactly one voltage pulse for every drive current pulse. In this article, we measure QLRs with respect to variations in the I_{dc} magnitude and I_{ac} peak pulse amplitude. If these parameters exceed the QLR, one or more JJs in the array will no longer generate a voltage pulse for each drive current pulse. We detect missing or extraneous pulses in the frequency domain by measuring both the amplitude of the synthesized voltage and the surrounding spectra. Within the QLR, the amplitude and spectral purity do not change as we vary a drive or bias parameter. We emphasize that a number of effects can lead to systematic errors within the QLR: the bias parameters affect the timing and shape of the JJ pulses, and the drive pulse feedthrough changes with the I_{ac} pulse amplitude. Therefore, for metrological purposes, any unintended changes in the amplitude and spectral purity within the QLRs will have to be included in an uncertainty budget.

A. QLR Measurement Setup

The QLR measurement setup is shown in Fig. 9. The AWG, RF amplifier, diplexer, and switch (SW) are the same as in the mixed-signal diagram (Fig. 5). The current source I_{dc} (Yokogawa FG401 isolated function generator) biases the JJs and an NI PXI-5922 24-bit digitizer is used to measure V_{JJ} for frequencies up to 1 MHz. Both instruments are connected to the corresponding $I_{\pm}$ and $V_{\pm}$ contacts of the JJ array in a four-probe configuration, as shown in Fig. 9.

The QLRs at 10 kHz were obtained by changing either the dc-bias current or the AWG's programmed pulse amplitude while digitizing the voltage across the JJ array at 1 MSa/s. We then evaluated the magnitude of the 10-kHz tone and the spectral purity as a function of either the bias or drive parameter. The dc-bias QLR can be measured quickly and

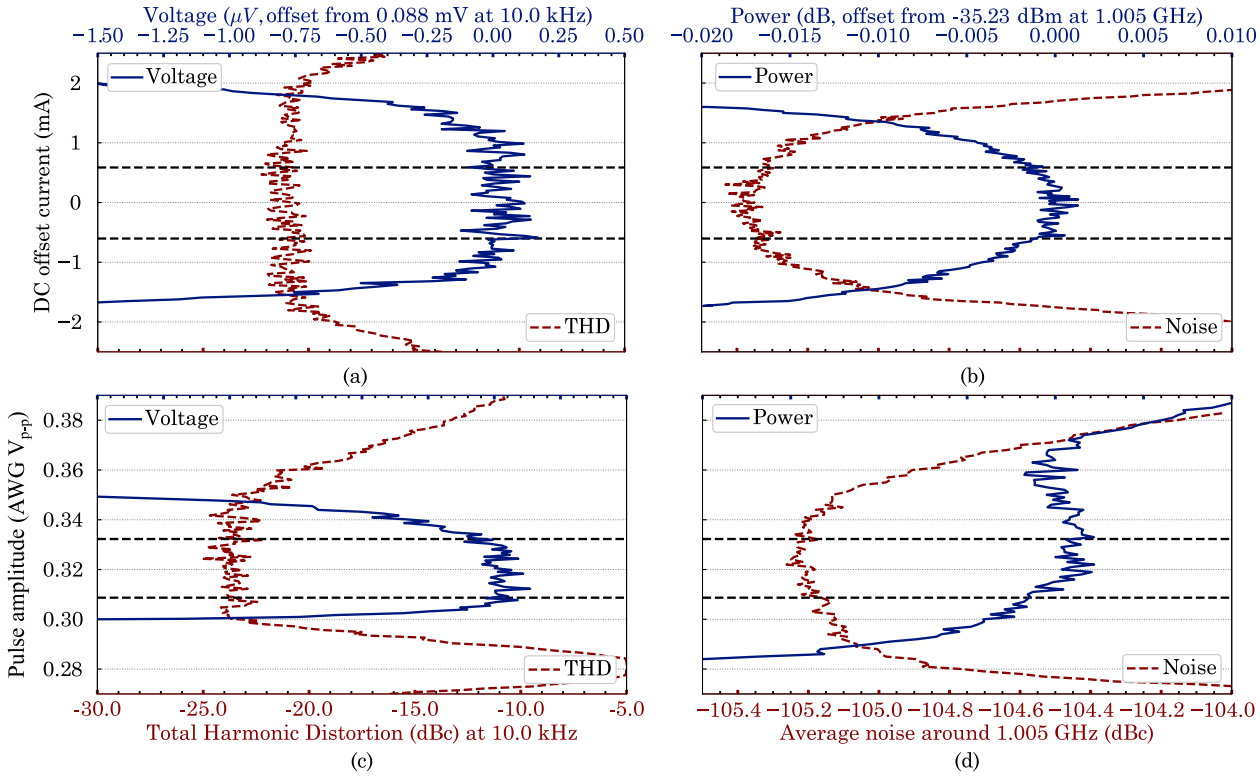

Fig. 10. (a) and (b) 10-kHz and 1.005-GHz QLR versus dc bias I_{dc} and (c) and (d) programmed AWG peak-to-peak amplitude. The dc-bias QLRs are measured at a 0.325-V_{p-p} AWG amplitude and the pulse-amplitude QLRs are measured at $I_{dc} = 0$. The horizontal black dashed lines show the QLR margins. The differences in THD and average noise in (a) versus (c) and (b) versus (d) are a result of the long-term drift in the measurement setup since measurements were done on different days.

accurately by applying I_{dc} as a triangular ramp at 1 Hz and digitizing an entire period of the ramp in a single digitizer acquisition [21].

We used this time-efficient low-frequency dc-bias QLR measurement to perform a manual, adaptive optimization of the EQ2 taps. The symmetrization procedure from Section III does not account for the signal path between the top of the dewar at room temperature and the 4500-JJ array. We reduce the effect of this path by tuning the 16-tap real-time FIR filter EQ2 (Fig. 5). In past work, this QLR-based manual equalization technique was used to compensate for the distortion of the entire signal path [8], [20], [21].

The synthesized microwave signal was measured at the LP diplexer port after being attenuated by 6 dB at the "RF Out" cable. The 6-dB attenuator reduces the return loss at the diplexer input and, therefore, the VSWR of the drive current along the JJ array. The spectra around the synthesized 1.005-GHz tone were measured by a Rohde & Schwarz FSV-7 signal analyzer. The spectra were acquired with 2-Hz resolution and video bandwidths for each dc current point produced by I_{dc} [2] or each pulse-amplitude point produced by the AWG.

We measured the feedthrough signal at 1.005 GHz using the SW in the state shown by the dashed lines in Fig. 9 and a 20-dB attenuator. The input–output signals at the AWG and amplifier are thus unchanged during both measurements, and the JJs respond nearly linearly to the 20-dB attenuated drive current (i.e. they do not pulse). In this configuration, we measured a −130-dBm signal at 1.005 GHz that was entirely due to the feedthrough of the drive current. After considering the attenuator, the feedthrough estimate at 1.005 GHz is −110 dBm. The QLRs were then measured with the SW in the state shown by the solid lines. Specifically, we show that this pattern of drive pulses forces each JJ to create a single voltage pulse per drive pulse by measuring both the dc-bias and pulse-amplitude QLRs at both 10 kHz and 1.005 GHz.

B. QLR Measurement Results

The dc-bias and pulse-amplitude QLR measurements around 10 kHz and 1.005 GHz are shown in Fig. 10. The rms voltage amplitude of the 10-kHz tone and its total harmonic distortion (THD) up to 500 kHz are the two metrics used to quantify the low-frequency QLR [8], [21]. The power of the 1.005-GHz tone and the average noise within ±250 kHz of the tone are the two metrics used to quantify the microwave-frequency QLR [2], [17].

We obtained a QLR over a dc-bias range greater than 1 mA at an AWG amplitude of 0.325 V_{p-p} [Fig. 10(a) and (b)] and a fractional pulse-amplitude range greater than 7.1% at 0-mA dc-bias current [Fig. 10(c) and (d)]. Over these ranges, the low-frequency THD and rms voltage do not depend on the bias or the drive parameter and are constant to better than 2 dB for the THD and better than 0.3 μV for the rms voltage. The 1.005-GHz noise and tone power are essentially constant with a flatness better than 0.3 dB for the noise and better than 0.003 dB for the tone power. Outside of these ranges, the curved dependencies indicate missing or extraneous JJ voltage pulses in response to the drive signal.

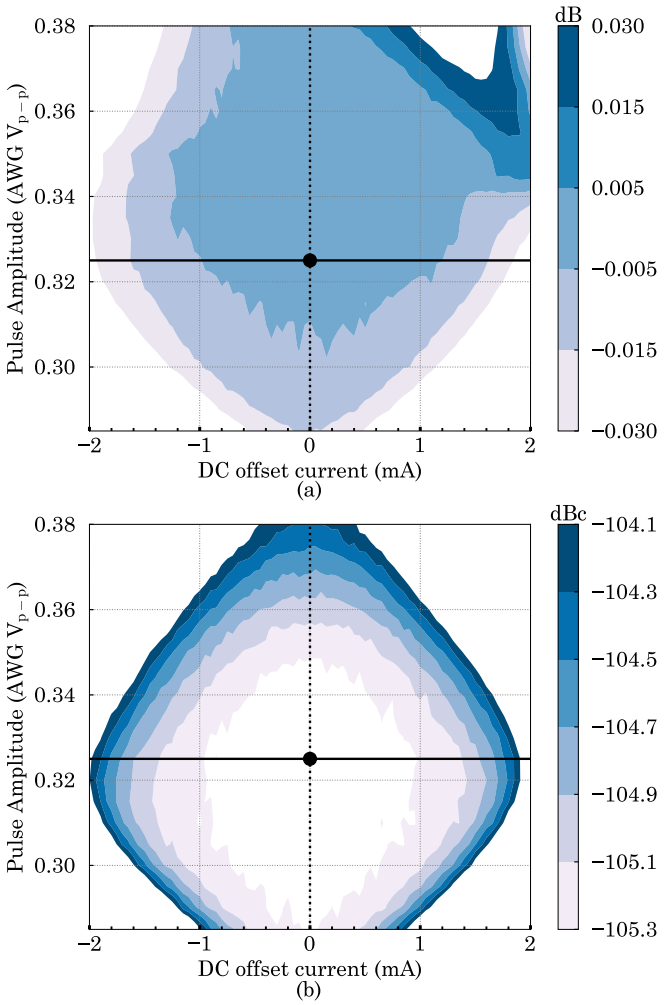

Fig. 11. Combined dc-bias and pulse-amplitude QLRs for the synthesized 1.005-GHz tone in terms of (a) tone power deviation and (b) average noise. The dc-bias sweep in Fig. 10(b) follows the horizontal solid lines and the pulse-amplitude sweep in Fig. 10(d) follows the dotted vertical lines. The circle at the intersection is the default optimal setting of 0.325-V_{p-p} AWG amplitude and $I_{dc} = 0$.

We expanded the microwave QLR measurements into a 2-D sweep over both the dc-bias and the pulse amplitude, as shown in Fig. 11. The tone power and average noise are dependent, which results in a roughly elliptical combined QLR. The values of the parameters used for the detailed sweeps in Fig. 10 are shown as lines in Fig. 11.

C. Spectra Around 1.005-GHz Tone

To better characterize the RF-JAWS source, we present the detailed spectra around 1.005 GHz in Fig. 12, which were acquired with the same default drive and bias values used in Fig. 10. A spectrum over a 100-MHz bandwidth on an 8-kHz grid is shown in Fig. 12(a). The expected transition from the delta–sigma digitization noise (see Fig. 4(c) to the signal analyzer noise floor is evident at 1.005 GHz ± 10 MHz. The additional spurs in this range are likely due to instrumentation IMD products.

The 1.005-GHz QLR data have been plotted using the power measured at the signal analyzer, but here, we also comment on the power at the JJ array. Ideally, we would perform an

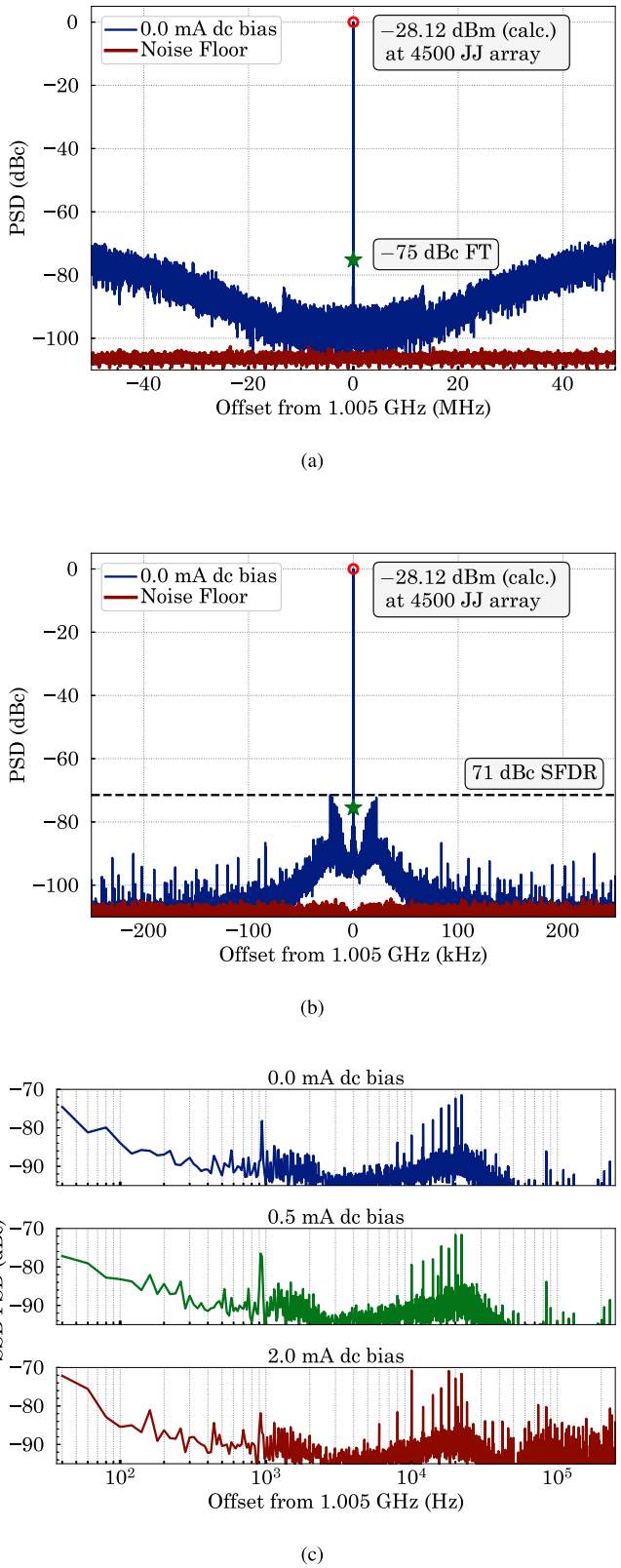

Fig. 12. (a) and (b) Spectra of the synthesized 1.005 GHz and the noise floor signal, both normalized to the 1.005-GHz peak. The feedthrough estimate ("−75-dBc FT" in (a), star) was calculated as explained in the main text. (c) Sample upper sideband spectra around the RF fundamental for different dc-bias currents. All spectra correspond to the default bias and drive settings from Fig. 10.

TABLE I

COMPARISON OF JJ-BASED AC AND RF VOLTAGE SOURCES. MAXIMAL AVAILABLE POWER ($\mathbf{P}_{\max}$) AND FEEDTHROUGH ARE MEASURED AT THE MAXIMAL SYNTHESIS FREQUENCY $\mathbf{f_t}$, ASSUMING NOMINAL LOAD AND MAXIMAL OPEN-CIRCUIT (O.C.) VOLTAGE

Reference [#] / Year	Topology One-/Two-port	Delta-Sigma Modulation Low-/Band-Pass	f_t (MHz)	Max. o.c. Voltage (mV rms)	Nominal Load (Ω)	P_{max} (dBm)	Feedthrough (dBc)
[7], [12] / 2020, 2018	One-port	Low-pass	0-0.1	4,000.00	1M	-18	< -90
[11] / 2020	One-port	Low-pass	0-0.5	1,000.00	1M	-30	< -90
[2] / 2020	Two-port	Band-pass	950-1050	1.59	50	-49	-40
[17] / 2020	One-port	Band-pass	10-1000	1.59	50	-49	-71
This Work	**Two-port**	**Low- and Band-pass**	**0-1005**	**17.56**	**50**	**-28**	**-75**

S-parameter error correction to the 4 K on-chip reference plane next to the 4500-JJ array. This is ongoing research [17] and is beyond the scope of this article. Instead, we calculate the expected power delivered to a DUT in an idealized 50-Ω environment, where $Z_S = Z_L = 50\ \Omega$ and the on-chip impedances in Fig. 2 are neglected. For the synthesized open-circuit rms voltage at 1.005 GHz of 17.56 mV, the power delivered to a $Z_L = 50\ \Omega$ load is -28.12 dBm (Fig. 12). This power is 7.11 dB larger than that measured at the signal analyzer Fig. 10. This is consistent with the estimated loss of the cryogenic coaxial cabling, mismatches of the signal analyzer, as well as the 6.62-dB total loss of the attenuator and diplexer measured with the VNA.

To evaluate the SFDR and spurious tones near the 1.005-GHz peak, we plot spectra over a 500-kHz bandwidth on a 20-Hz frequency grid [Fig. 12(b)]. We observe a 71-dBc SFDR that is limited by spurs that occur within ± 30 kHz of 1.005 GHz. To further investigate these spurs, we plot the measured upper sideband power spectral densities (PSDs) from 40 Hz to 250 kHz on a 20-Hz grid for $I_{\rm dc} = 0$, 0.5, and 2.0 mA in Fig. 12(c). The noise background and most of the spurs do not change at $I_{\rm dc} \leq 0.5$ mA. At offset frequencies below 900 Hz, we observe phase noise on the order of -85 dBc/Hz at a 100-Hz offset. The peak at an offset of 900 Hz is thought to come from low-frequency instrumentation noise picked up by the drive current signal path and upconverted by the nonlinear JJs. The spurs at even-frequency offsets from 6 to 24 kHz are most likely upconverted IMD products of the instrumentation at the 2-kHz repetition rate. There is a distinct difference between the spectra at the two quantum-locking biases $I_{\rm dc} = 0$ mA and 0.5 mA and the spectrum taken outside the QLR at 2.0 mA. Specifically, we observe additional spurious tones at harmonics of both the 2-kHz repetition rate and the 10-kHz synthesized tone. Bias noise can also cause the JJs to randomly pulse incorrectly, but in practice, these harmonic tones dominate the increase in the QLR noise metric.

V. CONCLUSION

We have demonstrated, for the first time, a quantum-based superconducting microwave voltage source with an open-circuit rms voltage amplitude exceeding 10 mV. We have developed a new approach for single-pulse zero-forcing symmetrization to compensate for room-temperature signal path distortion, which significantly improves the RF-JAWS performance. Table I shows a comparison of our work with other state-of-the-art JJ-based ac and RF voltage sources. As seen in the table, the results presented in this work are similar to [17] in terms of available synthesis frequencies and feedthrough levels. However, the demonstrated equalization scheme has enabled a 21-dB increase in the amplitude of quantum-based voltages, i.e., 17.56-mV rms open-circuit voltage at 1.005 GHz compared to the largest 1.59-mV rms at 1 GHz reported to date. This in turn has improved the SNR and SFDR, which is a substantial step toward creating application-ready microwave voltage/power standards. In order to suppress parasitic feedthrough voltages, we apply a combination of digital and analog HPFs to the drive signal. The latter causes significant drive pulse distortion, which limits the pulse-repetition frequency and, therefore, the amplitudes of the synthesized waveforms. The drive pulse equalization compensates for this distortion and enables higher waveform amplitudes while still suppressing the feedthrough error. Finally, we have demonstrated a two-tone approach for measuring the QLRs of the RF-JAWS and optimizing the drive pulses using the time-efficient measurements of low-frequency dc-bias QLR as the metric.

In the future, we need to further characterize RF-JAWS and continue to simplify and improve the equalization of the drive pulses. Along with the cryogenic signal path error correction, another important remaining characterization is that of the long-term stability of RF-JAWS, which includes the long-term amplitude and phase drift of the room-temperature and cryogenic devices and instruments. We would also like to assess the linear and nonlinear distortion of the room-temperature instrumentation to identify the sources of and minimize that distortion. Another topic of interest is the impact of bias pulse shape variation on the RF-JAWS system. Specifically, equalization can be used to reduce the width of the drive current pulses and thereby increase the upper limit of the synthesis frequency. Measurements of the pulse shape that have been calibrated to the on-chip reference plane will allow for improved distortion compensation [18], higher drive current pulse densities, and eventually an increase in the amplitudes of synthesized quantum-based arbitrary waveforms.

ACKNOWLEDGMENT

The authors would like to thank the NIST Boulder Microfabrication Facility for the support in the fabrication of the superconducting Josephson arbitrary waveform synthesizer (JAWS) chips described in this work. This work is a contribution of the U.S. Government and is not subject to U.S. copyright.

REFERENCES

[1] R. A. Ginley, "Traceability for microwave power measurements: Past, present, and future," in *Proc. IEEE 16th Annu. Wireless Microw. Technol. Conf. (WAMICON)*, Apr. 2015, pp. 1–5.

[2] C. A. Donnelly *et al.*, "1 GHz waveform synthesis with Josephson junction arrays," *IEEE Trans. Appl. Supercond.*, vol. 30, no. 3, pp. 1–11, Apr. 2020.

[3] P. F. Hopkins *et al.*, "RF waveform synthesizers with quantum-based voltage accuracy for communications metrology," *IEEE Trans. Appl. Supercond.*, vol. 29, no. 5, pp. 1–5, Aug. 2019.

[4] *Long-Term Evolution (LTE)*, Release 8, 3GPP, 2020. [Online]. Available: https://www.3gpp.org/specifications/releases/72-release-8

[5] *Long-Term Evolution (LTE) Advanced*, Release 10, 3GPP, 2020. [Online]. Available: https://www.3gpp.org/specifications/releases/70-release-10

[6] *5G New Radio*, Release 15, 3GPP, 2020. [Online]. Available: https://www.3gpp.org/release-15

[7] N. E. Flowers-Jacobs, A. Rufenacht, A. E. Fox, P. D. Dresselhaus, and S. P. Benz, "Calibration of an AC voltage source using a Josephson arbitrary waveform synthesizer at 4 V," in *Proc. Conf. Precis. Electromagn. Meas. (CPEM)*, Aug. 2020, pp. 1–2.

[8] N. E. Flowers-Jacobs, A. E. Fox, P. D. Dresselhaus, R. E. Schwall, and S. P. Benz, "Two-volt Josephson arbitrary waveform synthesizer using Wilkinson dividers," *IEEE Trans. Appl. Supercond.*, vol. 26, no. 6, pp. 1–7, Sep. 2016.

[9] O. F. Kieler, J. Kohlmann, R. Behr, F. Muller, L. Palafox, and J. Niemeyer, "SNS Josephson junction series arrays for the Josephson arbitrary waveform synthesizer," *IEEE Trans. Appl. Supercond.*, vol. 17, no. 2, pp. 187–190, Jun. 2007.

[10] O. F. Kieler, R. Iuzzolino, and J. Kohlmann, "Sub-μm SNS Josephson junction arrays for the Josephson arbitrary waveform synthesizer," *IEEE Trans. Appl. Supercond.*, vol. 19, no. 3, pp. 230–233, Jun. 2009.

[11] M. Kraus *et al.*, "Measurement and analysis of high-frequency voltage errors in the Josephson arbitrary waveform synthesizer," *Meas. Sci. Technol.*, vol. 31, no. 12, Dec. 2020, Art. no. 125003.

[12] J. M. Underwood, "Uncertainty analysis for AC–DC difference measurements with the AC Josephson voltage standard," *Metrologia*, vol. 56, no. 1, p. 15012, 2018.

[13] T. M. Wallis, T. P. Crowley, D. X. LeGolvan, and R. A. Ginley, "A direct comparison system for power calibration up to 67 GHz," in *Proc. Conf. Precis. Electromagn. Meas.*, Jul. 2012, pp. 726–727.

[14] J. X. Przybysz *et al.*, "Josephson junction digital to analog converter for accurate AC waveform synthesis," U.S. Patent 5 812 078, Sep. 22, 1998.

[15] S. Benz and C. Hamilton, "A pulse-driven programmable Josephson voltage standard," *Appl. Phys. Lett.*, vol. 68, no. 22, pp. 3171–3173, May 1996, doi: 10.1063/1.115814.

[16] S. P. Benz, C. A. Hamilton, C. J. Burroughs, T. E. Harvey, L. A. Christian, and J. X. Przybysz, "Pulse-driven Josephson digital/analog converter [voltage standard]," *IEEE Trans. Appl. Supercond.*, vol. 8, no. 2, pp. 42–47, Jun. 1998.

[17] J. A. Brevik *et al.*, "Cryogenic calibration of the RF Josephson arbitrary waveform synthesizer," in *Proc. Conf. Precis. Electromagn. Meas. (CPEM)*, Aug. 2020, pp. 1–2.

[18] A. S. Boaventura *et al.*, "Cryogenic calibration of a quantum-based radio frequency source," in *Proc. 95th Microw. Meas. Conf. (ARFTG)*, Aug. 2020, pp. 1–4.

[19] C. Donnelly, "Development of a quantum-based superconducting radio-frequency voltage standard," Ph.D. dissertation, Dept. Elect. Eng., Stanford Univ., Stanford, CA, USA, Mar. 2019.

[20] N. E. Flowers-Jacobs, S. B. Waltman, A. E. Fox, P. D. Dresselhaus, and S. P. Benz, "Josephson arbitrary waveform synthesizer with two layers of Wilkinson dividers and an FIR filter," *IEEE Trans. Appl. Supercond.*, vol. 26, no. 6, pp. 1–7, Sep. 2016.

[21] N. E. Flowers-Jacobs, A. A. Babenko, A. E. Fox, J. A. Brevik, P. D. Dresselhaus, and S. P. Benz, "Zero-compensation Josephson arbitrary waveform synthesizer at 1.33 V," in *Proc. Conf. Precis. Electromagn. Meas. (CPEM)*, Aug. 2020, pp. 1–2.

[22] T. V. Duzer and C. W. Turner, *Principles of Superconductive Devices and Circuits*, 2nd ed. Upper Saddle River, NJ, USA: Prentice-Hall, 1999, ch. 4.

[23] C. A. Donnelly, J. A. Brevik, P. D. Dresselhaus, P. F. Hopkins, and S. P. Benz, "Jitter sensitivity analysis of the superconducting Josephson arbitrary waveform synthesizer," *IEEE Trans. Microw. Theory Techn.*, vol. 66, no. 11, pp. 4898–4909, Nov. 2018.

[24] G. T. S. Pavan and R. Schreier, *Understanding Delta-Sigma Data Converters*, 2nd ed. Hoboken, NJ, USA: Wiley, 2017.

[25] C. A. Donnelly *et al.*, "Quantized pulse propagation in Josephson junction arrays," *IEEE Trans. Appl. Supercond.*, vol. 30, no. 3, pp. 1–8, Apr. 2020.

[26] B. Baek, P. D. Dresselhaus, and S. P. Benz, "Co-sputtered amorphous Nb_xSi_{1-x} barriers for Josephson-junction circuits," *IEEE Trans. Appl. Supercond.*, vol. 16, no. 4, pp. 1966–1970, Dec. 2006.

[27] M. Elsbury, "Broadband microwave integrated circuits for voltage standard applications," Ph.D. dissertation, Dept. Elect. Comput. Eng., Univ. Colorado, Boulder, CO, USA, Jan. 2010.

[28] B. Xavier, *Ultra Wide Band Antennas*, 2nd ed. Hoboken, NJ, USA: Wiley, 2011, ch. 3.

[29] K. J. Coakley and P. Hale, "Alignment of noisy signals," *IEEE Trans. Instrum. Meas.*, vol. 50, no. 1, pp. 141–149, Feb. 2001.

[30] H. E. Kallmann, "Transversal filters," *Proc. IRE*, vol. 28, no. 7, pp. 302–310, Jul. 1940.

[31] R. D. Gitlin and S. B. Weinstein, "Fractionally-spaced equalization: An improved digital transversal equalizer," *Bell Syst. Tech. J.*, vol. 60, no. 2, pp. 275–296, Feb. 1981.

[32] E. L. Ginzton, W. R. Hewlett, J. H. Jasberg, and J. D. Noe, "Distributed amplification," *Proc. IRE*, vol. 36, no. 8, pp. 956–969, Aug. 1948.

[33] G. Nikandish, R. B. Staszewski, and A. Zhu, "The (R)evolution of distributed amplifiers: From vacuum tubes to modern CMOS and GaN ICs," *IEEE Microw. Mag.*, vol. 19, no. 4, pp. 66–83, Jun. 2018.

[34] A. Monmayrant, S. Weber, and B. Chatel, "A newcomer's guide to ultrashort pulse shaping and characterization," *J. Phys. B, At., Mol. Opt. Phys.*, vol. 43, no. 10, May 2010, Art. no. 103001, doi: 10.1088/0953-4075/43/10/103001.

[35] G. E. Bottomley, *Channel Equalization for Wireless Communications: From Concepts to Detailed Mathematics*. Piscataway, NJ, USA: IEEE Press, 2011.

[36] S. Benedetto and E. Biglieri, "Nonlinear equalization of digital satellite channels," *IEEE J. Sel. Areas Commun.*, vol. SAC-1, no. 1, pp. 57–62, Jan. 1983.

[37] N. L. Peccarelli and C. Fulton, "Adaptive nonlinear equalization for digital array receivers," *IEEE Trans. Microw. Theory Techn.*, vol. 67, no. 11, pp. 4493–4504, Nov. 2019.

Akim A. Babenko (Graduate Student Member, IEEE) received the B.S. degree (Hons.) in electronics and nanoelectronics and the M.S. degree (Hons.) in radiophysics from Kuban State University, Krasnodar, Russia, in 2017 and 2019, respectively. He is currently pursuing the Ph.D. degree at the National Institute of Standards and Technology, Boulder, CO, USA, on the Quantum Voltage Project. His B.S. and M.S. research was on the vector network analysis of microwave mixers.

Upon graduation in 2017, he did a summer internship at Fermilab, Batavia, IL, USA, developing DSP firmware for superconducting accelerating RF cavities. He joined Prof. Popovic's group at the University of Colorado, Boulder, in Fall 2018. He works on designing multidecade bandwidth passive and active monolithic microwave integrated circuits (MMICs) in III–V and superconductor technologies, as well as developing new measurement and signal processing techniques for RF Josephson arbitrary waveform synthesizes.

Nathan E. Flowers-Jacobs (Member, IEEE) was born in Urbana, IL, USA, in June 1979. He received the B.S. degree in physics from the California Institute of Technology, Pasadena, CA, USA, in 2001, and the Ph.D. degree in physics from JILA, Boulder, CO, USA, and the University of Colorado at Boulder, Boulder, CO, USA, in 2010, with a focus on a quantum-limited detector of nanomechanical motion based on electron tunneling across an atomic point contact.

He worked at the MIT Lincoln Laboratory, Lexington, MA, USA, modeling radar cross sections for two years before his Ph.D. degree. From 2010 to 2014, he was a Post-Doctoral Associate at Yale University, New Haven, CT, USA, working on nanomechanical displacement measurements at the quantum limit using optical cavities. In 2014, he joined the Quantum Voltage Project at the National Institute of Standards and Technology (NIST), Boulder, CO, USA, and has been working on the development, characterization, and applications of the Josephson arbitrary waveform synthesizer (JAWS), an ac Josephson voltage standard based on pulse-biased arrays of Josephson junctions.

Dr. Flowers-Jacobs received the IEEE Council on Superconductivity Van Duzer Prize in 2019.

Gregor Lasser (Member, IEEE) received the Dipl.-Ing. and Dr. Techn. degrees (Hons.) in electrical engineering from the Vienna University of Technology, Vienna, Austria, in 2008 and 2014, respectively.

Since 2017, he has been an Assistant Research Professor with the University of Colorado at Boulder, Boulder, CO, USA, where he is working on broadband supply-modulated power amplifiers and compact intelligent antenna systems.

Dr. Lasser received the second position of the EEEfCOM Innovation Award in 2008 for the RFID testbed developed during his diploma thesis and the Faculty Award of the Faculty of Electrical Engineering and Information Technology, Vienna University of Technology, for the presentation of his Doctoral dissertation entitled "Passive RFID for Automotive Sensor Applications." In 2017, he received the Best Paper Award at IEEE WAMICON for his work on analog predistortion of GaN power amplifiers. Since 2016, he has been serving as the Vice Chair for the IEEE Denver Joint AP-S/MTT Section.

Justus A. Brevik (Member, IEEE) received the B.S. degree in physics from the University of Washington, Seattle, WA, USA, in 2002, and the Ph.D. degree in physics from the California Institute of Technology, Pasadena, CA, USA, in 2012, with a focus on the measurement of cosmic microwave background polarization using the BICEP2 telescope.

He joined the National Institute of Standards and Technology (NIST), Boulder, CO, USA, as a National Research Council Fellow in 2012, where he worked on transition-edge sensor (TES) detectors and microwave superconducting quantum interference device multiplexer for astrophysics applications. In 2014, he joined a startup company attempting to launch thermal rockets into space using beamed microwave power generated by gyrotrons. He returned to NIST Boulder in 2015 to work in the Quantum Voltage Project, where he is developing a Josephson arbitrary waveform synthesizer capable of creating quantum-accurate waveforms in the gigahertz regime for telecommunications and quantum information applications.

Dr. Brevik received the IEEE Council on Superconductivity Van Duzer Prize in 2019.

Anna E. Fox (Senior Member, IEEE) received the Ph.D. degree in electrical engineering from Drexel University, Philadelphia, PA, USA, in 2009.

From 2009 to 2010, she was a National Research Council Post-Doctoral Researcher at the Optoelectronics Division, National Institute of Standards and Technology, Boulder, CO, USA, where she worked fabricating superconducting transition-edge sensor (TES) for use at optical wavelengths. She continued her work in TES fabrication in the NIST Quantum Sensors Project, where she fabricated arrays of TES bolometers for cosmic microwave background detection. Since 2013, she has been with the NIST Quantum Voltage Project, pursuing the design and fabrication of voltage standard devices such as the programmable Josephson voltage standard and the ac Josephson voltage standard.

Dr. Fox received the 2016 and 2019 IEEE Council on Superconductivity Van Duzer Prize.

Paul D. Dresselhaus was born in Arlington, MA, USA, in January 1963. He received the B.S. degree in physics and electrical engineering from the Massachusetts Institute of Technology, Cambridge, MA, USA, in 1985, and the Ph.D. degree in applied physics from Yale University, New Haven, CT, USA, in 1991.

In 1999, he joined the Quantum Voltage Project, National Institute of Standards and Technology, Boulder, CO, USA, where he has been developing novel superconducting circuits and broadband bias electronics for precision voltage waveform synthesis and programmable voltage standard systems. He has been the Project Leader of the Quantum Voltage Project at NIST since October 2015. He was with Northrop Grumman, Denver, CO, USA, for three years, where he designed and tested numerous gigahertz-speed superconductive circuits, including code generators and analog-to-digital converters. He also upgraded the simulation and layout capabilities at Northrop Grumman to be among the world's best. He has also been a Post-Doctoral Assistant with the State University of New York, Stony Brook, NY, USA, where he worked on the nanolithographic fabrication and study of Nb–AlO_x–Nb junctions for single-electron and single flux quantum (SFQ) applications, single-electron transistors and arrays in Al–AlO_x tunnel junctions, and the properties of ultrasmall Josephson junctions.

Dr. Dresselhaus received two U.S. Department of Commerce Gold Medals for Distinguished Achievement and the IEEE Council on Superconductivity Van Duzer Prize in 2006, 2016, and 2019.

Zoya Popović (Fellow, IEEE) received the Dipl.-Ing. degree from the University of Belgrade, Belgrade, Serbia, in 1985, and the Ph.D. degree from Caltech, Pasadena, CA, USA, in 1990.

She was a Visiting Professor with the Technical University of Munich, Munich, Germany, from 2001 to 2003; and ISAE, Toulouse, France, in 2014. She was the Chair of Excellence at Carlos III University, Madrid, Spain, from 2018 to 2019. She is currently a Distinguished Professor and the Lockheed Martin Endowed Chair in Electrical Engineering at the University of Colorado at Boulder, Boulder, CO, USA. She has graduated over 65 Ph.D. students and currently advises 17 doctoral students. Her research interests are in high-efficiency power amplifiers and transmitters, microwave and millimeter-wave high-performance circuits for communications and radar, medical applications of microwaves, quantum sensing and metrology, and wireless powering.

Dr. Popović was a recipient of two IEEE MTT Microwave Prizes for best journal articles, the White House NSF Presidential Faculty Fellow Award, the URSI Issac Koga Gold Medal, the ASEE/HP Terman Medal, and the German Alexander von Humboldt Research Award. She was elected as a foreign member of the Serbian Academy of Sciences and Arts in 2006. She was named the IEEE MTT Distinguished Educator in 2013 and the University of Colorado Distinguished Research Lecturer in 2015.

Samuel P. Benz (Fellow, IEEE) was born in Dubuque, IA, USA, in December 1962. He received the B.A. degree *(summa cum laude)* in physics and math from Luther College, Decorah, IA, USA, in 1985, and the M.A. and Ph.D. degrees in physics from Harvard University, Cambridge, MA, USA, in 1987 and 1990, respectively.

In 1990, he joined the National Institute of Standards and Technology (NIST), Boulder, CO, USA, as a NIST/NRC Postdoctoral Fellow and became a permanent Staff Member in January 1992. He has been the Project Leader of the Quantum Voltage Project at NIST since October 1999 and the Group Leader of the Superconductive Electronics Group since 2015. He has worked on a broad range of topics within the field of superconducting electronics, including Josephson junction array oscillators, single flux quantum (SFQ) logic, ac and dc Josephson voltage standards, Josephson waveform synthesis, and noise thermometry. He has over 290 publications. He holds four patents in the field of superconducting electronics.

Dr. Benz is a Fellow of NIST and the American Physical Society (APS). He is a member of Phi Beta Kappa and Sigma Pi Sigma. He has received three U.S. Department of Commerce Gold Medals for Distinguished Achievement, the 2016 IEEE Joseph F. Keithley Award, and the IEEE Council on Superconductivity Van Duzer Prize in 2006, 2016, and 2019. He was awarded an R. J. McElroy Fellowship from 1985 to 1988 to work toward the Ph.D. degree.